geosciences

MDPI

Article

Geochemical Characteristics of the Lower Cretaceous Luohe Formation in Xiaozhuang Coal Mine, China: New Insights into Its Provenance and Paleoenvironment

Yue Cai [1,2,3], Shiwu Liu [1,2,3], Liangliang He [4], Xiang Guo [4], Guijuan Li [4], Lei Yang [4] and Shaoni Wei [1,2,3,*]

[1] College of Geology and Environment, Xi'an University of Science and Technology, Xi'an 710054, China
[2] Key Laboratory of Coal Resources Exploration and Comprehensive Utilization, Ministry of Natural Resources, Xi'an 710026, China
[3] Shaanxi Province Key Laboratory of Geological Support for Coal Green Development, Xi'an University of Science and Technology, Xi'an 710054, China
[4] 186 Coalfield Geological Co., Xi'an 710065, China
* Correspondence: snwei@xust.edu.cn

Abstract

Sandstone of the Lower Cretaceous Luohe Formation is the main water inrush source in the Binchang Mining Area in the southwestern Ordos Basin. Its sedimentary environment and provenance features are critical for local coal development and safe mining. The Luohe Formation at Xiaozhuang Coal Mine comprises three vertical members: the lower member dominated by coarse- to medium-grained sandstones, the middle member mainly composed of fine-grained sandstones, and the upper member characterized by interbedded fine- to medium-grained sandstones and sandy conglomerates. This subdivision newly identifies a complete hydrodynamic evolutionary cycle of depositional environments from high-energy to low-energy and back to high-energy conditions. Integrated petrographic observations and analyses of major and rare earth elements first confirm that the tectonic affinity of the Luohe Formation progressively shifted from a passive continental margin to an active continental margin, accompanied by a corresponding transition in sediment provenance from the North China Craton to a magmatic arc source region. Trace element compositions precisely indicate that the Luohe Formation was deposited in a fluvial freshwater environment under hot, arid, and oxidizing conditions, thus providing new constraints on the paleoenvironmental evolution of the region.

Keywords: paleoenvironmental evolution; provenance; geochemistry; Luohe Formation; Ordos Basin

Check for updates

Academic Editor: Salvatore Critelli

Received: 28 January 2026
Revised: 3 April 2026
Accepted: 10 April 2026
Published: 21 April 2026

Copyright: © 2026 by the authors. Licensee MDPI, Basel, Switzerland. This article is an open access article distributed under the terms and conditions of the Creative Commons Attribution (CC BY) license.

1. Introduction

The Ordos Basin is one of the most coal-rich regions in China [1]. The Lower Cretaceous Luohe Formation (K_1l) of the Zhidan Group is widely distributed in the basin, dominated by thick-bedded sandstone deposits. It preserves key sedimentary evolution information of the Early Cretaceous [2], and serves as a core carrier for studying the tectono-sedimentary evolution process of the basin during this period. The Binchang Mining Area is located at the southwestern margin of the Ordos Basin. The thickness of the Luohe Formation in this area ranges from 200 to 400 m, with significant differences in water abundance, making it one of the main water inrush risk sources during coal mining. However, current studies on the Luohe Formation in the Binchang Mining Area are mostly focused

on hydrogeological characteristics and water hazard prevention engineering [3–5], while systematic research on its sedimentary environment and provenance-tectonic background is still lacking, which is inconsistent with the controlling effect of lithological assemblages and sedimentary characteristics on formation water abundance. Previous studies have shown that the Luohe Formation is widely distributed in the Ordos Basin and is mainly composed of fluvial and desert facies deposits [6–9]. Notably, the Binchang Mining Area is exactly located at the transitional zone between alluvial fan-braided river facies and desert dune facies [10–12]. Previous Cretaceous studies at the basin scale have been unable to accurately characterize the sedimentary and geochemical characteristics of this transitional zone, resulting in insufficient targeted understanding of the Luohe Formation in the study area and failure to fully support water hazard prevention and control in coal mining.

Taking the sandstones of the Luohe Formation in the Xiaozhuang Coal Mine of the Binchang Mining Area as the research object, this study aims to supplement the weak parts of the research on the sedimentary environment and provenance of the Luohe Formation in the transitional zone by integrating various analytical techniques, clarify its sedimentary evolution laws, provenance characteristics and tectonic background, and provide a scientific basis for regional coal resource development and safe coal mining.

Sedimentary rocks preserve abundant geochemical information. The integration of petrography, grain-size analysis, and major, trace, and rare earth element (REE) geochemistry provides a robust means of reconstructing depositional processes, tectonic setting, provenance, and paleoenvironmental conditions [13–19]. Major-element compositions can constrain compositional maturity and tectono-sedimentary setting, whereas relatively immobile trace elements and REEs are widely used to identify provenance and source-rock affinity [20–25]. In particular, sedimentary rocks derived from similar source regions commonly display comparable REE distribution patterns, making REE geochemistry a useful tool for provenance discrimination [15].

The southwestern margin of the Ordos Basin is adjacent to several potential source regions, including the North Qinling Orogenic Belt, the Alxa Block, and the northern margin of the North China Craton [26]. These source areas comprise different basement and magmatic rock assemblages, implying a complex source-to-sink system for the Luohe Formation in the Xiaozhuang area. Therefore, an integrated sedimentological and geochemical investigation is needed to clarify the vertical relationships among facies differentiation, provenance transition, and paleoenvironmental evolution within this thick sandstone succession.

In this study, grain-size analysis, petrographic observations, X-ray fluorescence spectroscopy (XRF), and inductively coupled plasma mass spectrometry (ICP-MS) are integrated to investigate the Luohe Formation in the Xiaozhuang Coal Mine. This study aims to (1) characterize the vertical depositional evolution of the formation; (2) investigate its provenance evolution, tectonic setting, and source-rock types; and (3) reconstruct its paleoenvironment in terms of paleoclimate, paleosalinity, and redox conditions.

2. Geological Background

2.1. Tectonic and Sedimentary Settings

Xiaozhuang Coal Mine is located in the central part of the Huanglong Jurassic Coalfield in Shaanxi Province, within the Binxian–Changwu County area, and forms part of the Binchang Mining Area. Tectonically, the mine is situated on the southwestern margin of the Ordos Basin, at the junction of the western segment of the Xunyi Depression (within the Shanbei Slope), the northern margin of the Weibei Uplift, and the eastern flank of the Western Fold Belt (Figure 1c) [26]. The southwestern basin margin represents a zone of complex tectonic interactions, with adjacent tectonic units including the North Qilian

Orogenic Belt, North Qinling Orogenic Belt, Alxa Block, and the northern margin of the North China Craton—all of which may have contributed to the sedimentary provenance of the study area [27]. This provides the tectonic framework for the multi-provenance sedimentary system of the Luohe Formation.

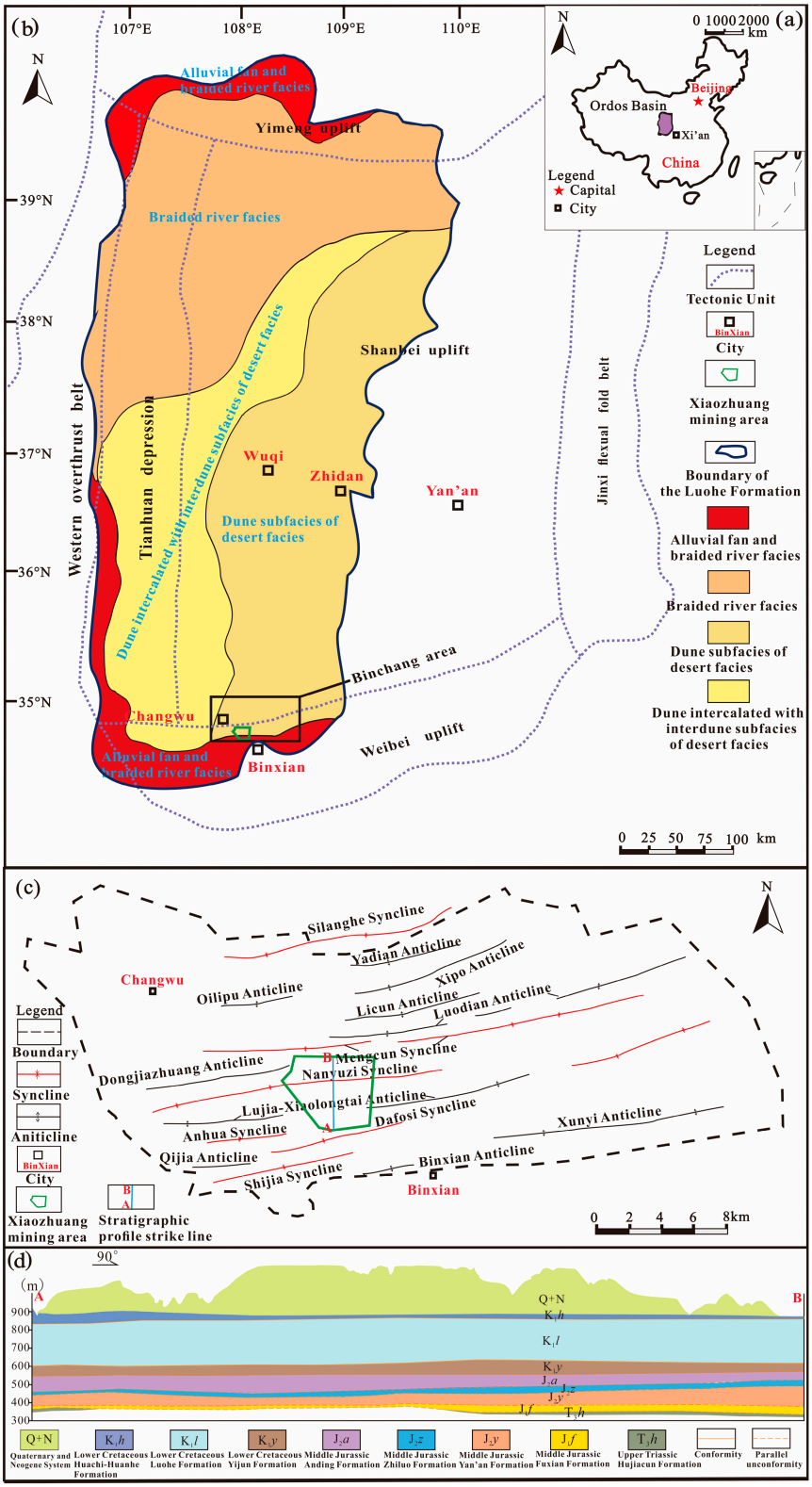


Figure 1. (**a**) Location of the Ordos Basin; (**b**) Distribution of Early Cretaceous strata and major tectonic units in the Ordos Basin; (**c**) Geological structure of the Xiaozhuang Coal Mine in the Binchang Mining Area; (**d**) North–south stratigraphic cross-section of the study area.

Within the depositional extent of the Cretaceous Luohe Formation in the Ordos Basin, with the exception of localized alluvial fan–braided river facies along the basin margin, the formation is predominantly composed of desert facies deposits (Figure 1b) [28,29]. The study area is situated at the transition between the alluvial fan–braided river facies and the dune subfacies of the desert system within the Luohe Formation [30]. The geological structure of the mining area is relatively simple, dominated by a gently northwest-dipping monocline, with minor folds—including short-axis anticlines and broad gentle synclines—developed locally. The fold axes generally trend NEE-SWW. Stratal dip angles are typically less than 10°, with relatively well-developed faulting [31].

2.2. Stratigraphic and Lithologic Characteristics

The stratigraphic sequence at Xiaozhuang Coal Mine, from bottom to top, consists of the Hujiacun Formation ($T_{2-3}h$), Fuxian Formation (J_1f), Yan'an Formation (J_2y), Zhiluo Formation (J_2z), Anding Formation (J_2a), Yijun Formation (K_1y), Luohe Formation (K_1l), Huachi Formation (K_1h) [32]. The location of the stratigraphic section is shown in Figure 1c, and the section itself is presented in Figure 1d.

The Lower Cretaceous Luohe Formation is conformably overlain by the Huachi Formation and underlain by the Yijun Formation. The sedimentary succession is complete, with a thickness ranging from 157.20 m to 330.59 m and an average of 268.30 m. In the studied XZ2102 borehole, the Luohe Formation is 330 m thick. Parallel bedding is observed in hand specimens XZ10 and XZ25. Based on sedimentary cycles (indicated by the red triangles denoting upward-shallowing cycles) and lithological associations, the Luohe Formation is subdivided into three members from bottom to top: (1) the lower member (146 m thick), consisting of interbedded fine- to medium-grained sandstones with intercalations of coarse sandstone; (2) the middle member (70 m thick), composed predominantly of fine and very fine sandstones; (3) the upper member (114 m thick), characterized by interbedded fine and medium-fine sandstones with sandy conglomerate intercalations (Figure 2). Casting thin sections were prepared for all thirty-three samples, and grain-size analysis was performed under a microscope. The cast thin sections were impregnated with red-dyed epoxy resin.

The Luohe Formation is dominated by lithic arkose with minor feldspathic lithic sandstone (Figures 3 and 4, The small circles in the figure represent the samples). Clastic grains account for 59–79% and are dominated by quartz, feldspar and lithic fragments, with minor mica. Quartz content ranges from 30–51%, including monocrystalline and polycrystalline quartz, with no secondary overgrowth or dissolution. Feldspar content is 9–20%, dominated by plagioclase and minor K-feldspar. Lithic fragments account for 10–22%, mainly igneous and metamorphic rock fragments. Interstitial materials vary significantly in content (5–20%) and are dominated by cements, including argillaceous ferruginous materials and ferrocalcite. The samples are moderately to well sorted, with grains dominated by subangular rounding. Clastic grains are dominated by point contacts, with local line contacts, and characterized by contact cementation.

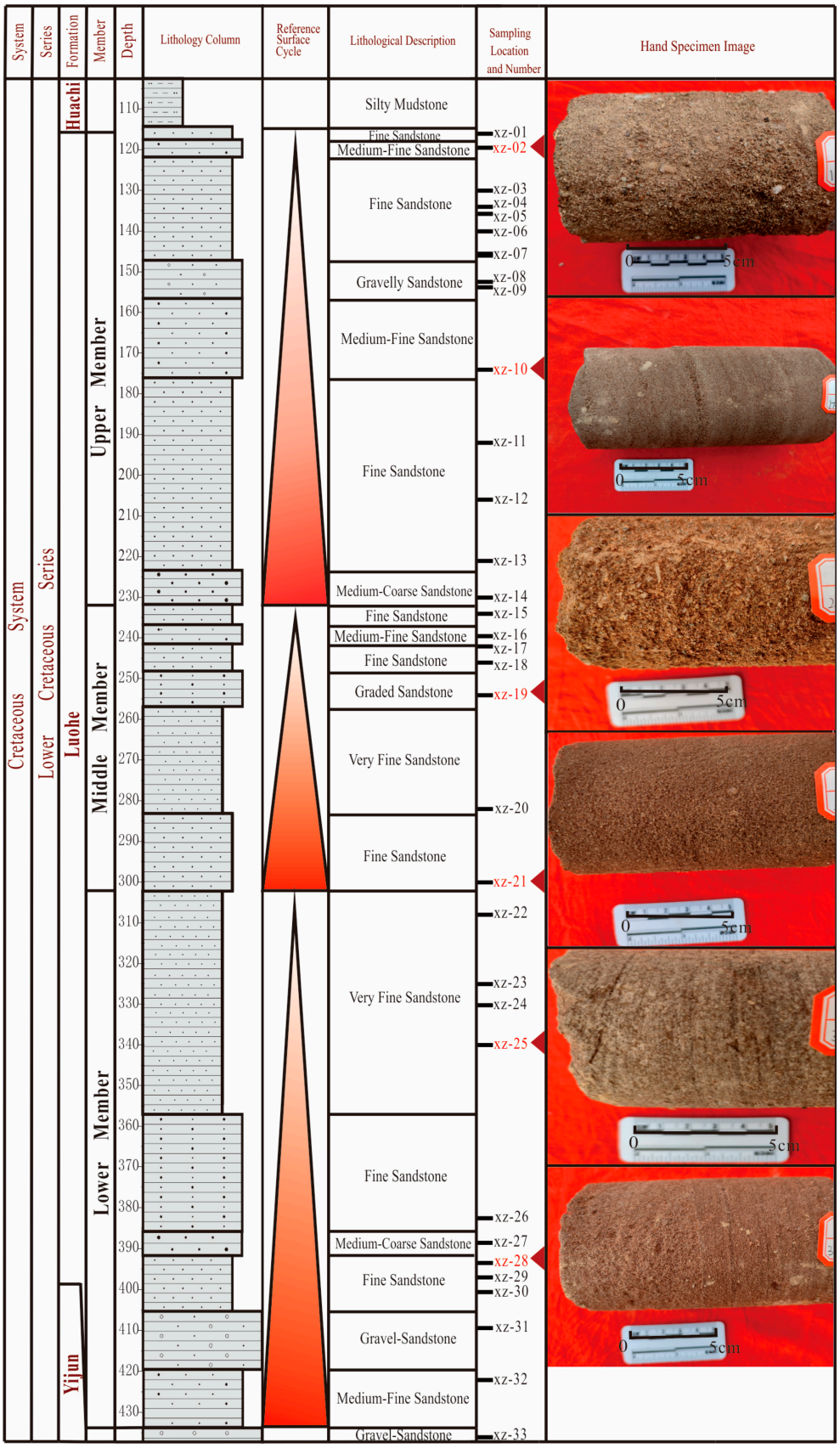


Figure 2. Lithological column of the Luohe Formation sandstone in Xiaozhuang Coal Mine, showing stratigraphic division, lithological associations, sedimentary cycles, sampling locations, and hand specimen images. The small triangles in the sampling position and number column indicate the sample numbers corresponding to the hand specimen images.

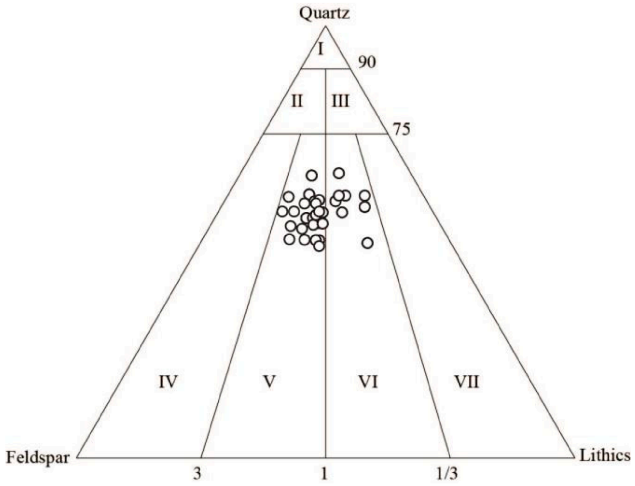


Figure 3. Lithofacies classification of the Luohe Formation sandstone in Xiaozhuang Coal Mine. I—Quartz arenite; II—Feldspathic quartz arenite; III—Lithic quartz arenite; IV—Arkose; V—Lithic arkose; VI—Feldspathic litharenite; VII—Litharenite.

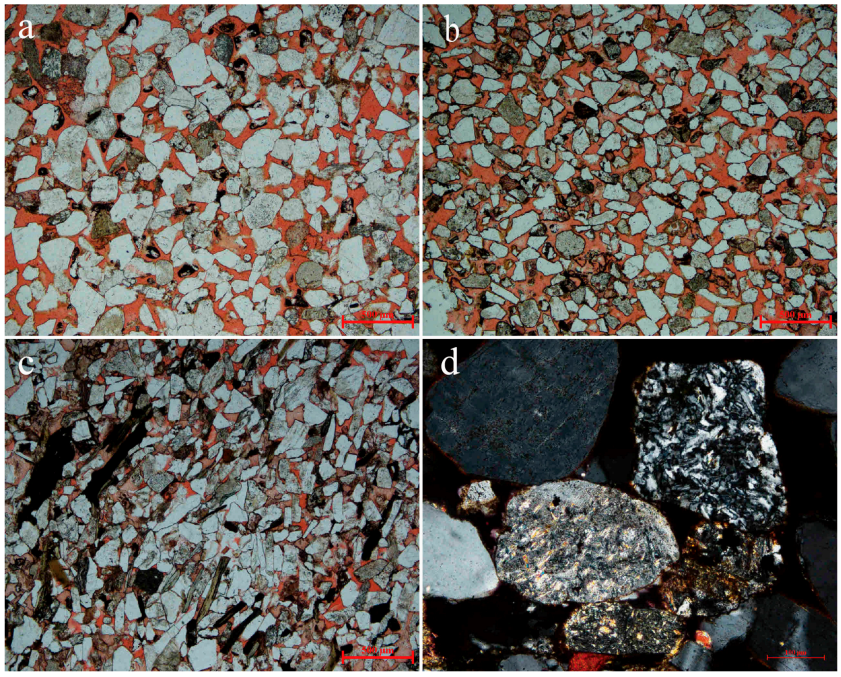


Figure 4. Microphotographs of the Luohe Formation sandstone in Xiaozhuang Coal Mine. (**a**) Fine-grained lithic arkose, well sorted, with subangular to subrounded grains; (**b**) Lithic arkose, moderately sorted, with well-developed pores; (**c**) Lithic fragments of biotite and muscovite are weakly oriented; intergranular spaces are filled with calcite and pelitic-ferruginous cements; (**d**) Igneous and metamorphic lithic fragments in feldspathic litharenite.

3. Experiment Methods and Results

3.1. Experiment Methods

Thirty-three representative samples were collected from the XZ2102 drill hole at Xiaozhuang Coal Mine, covering the entire Luohe Formation evenly in the vertical direction. During field sampling, complete and unweathered fresh cores were selected, and the weathered and broken surface layers were removed to ensure that the original characteristics of the samples remained undisturbed.

Lithological identification results indicate that the collected samples are dominated by purple–red and brown–red massive sandstones, encompassing three grain size categories:

coarse-grained, medium-grained, and fine-grained. To facilitate subsequent microscopic observations, one cast thin section was prepared for each core sample, totaling 33 sections. Seven typical microscopic fields of view were selected for each prepared polished thin section, which were observed individually, and a microscopic photograph was taken for each field of view to retain comprehensive microscopic characteristic data. Grain size analysis was performed in accordance with the industry standard SY/T 5368-2016 [33] "Methods for Identification of Rock Thin Sections", and a particle size image analysis software was employed to complete the systematic testing of the Luohe Formation samples from Xiaozhuang Coal Mine.

The analyses of major elements, trace elements, and rare earth elements in the sandstone samples were conducted in the professional laboratory of Xi'an Institute of Geology, Shaanxi, China, with the entire process strictly adhering to national standards and specifications. Their test principles, instrumental methods, analytical procedures, quality control requirements, and error limits are fully consistent with international standards and global geochemical norms. Major elements were determined using X-ray Fluorescence Spectrometer (XRF), Malvern Panalytical, Almelo, The Netherlands, in strict compliance with GB/T 14506.28-2010 [34] "Methods for Chemical Analysis of Silicate Rocks—Part 28: Determination of 16 Major and Minor Component Contents"; trace elements and rare earth elements were analyzed using an Elan 6100DRC Inductively Coupled Plasma Mass Spectrometer (ICP-MS), PerkinElmer, Waltham, MA, USA, in accordance with GB/T 14506.30-2010 [35] "Methods for Chemical Analysis of Silicate Rocks—Part 30: Determination of 44 Element Contents".

For experimental calibration and quality control, national first-class rock reference materials matching the matrix of the sandstone samples were selected for calibration, which fully meets the explicit requirements for analytical quality control specified in the above two national standards. The analysis error was monitored throughout the testing process: the analysis error of major elements was controlled within 5%, the analysis error of key trace elements and rare earth elements (including Co, Ni, Zn, Ga, Rb, Zr, Nb, Hf, La, Ce, Pr, Nd, Sm, and Eu) was less than 5%, and the analysis error of other elements was controlled within the range of 5% to 10%, ensuring the accuracy and reliability of the test data.

3.2. Results

3.2.1. Granulometric Analysis

The grain-size analysis of the samples yields a mean value of 2.30 φ (range: −0.82 to 3.40 φ), corresponding to an actual particle size of approximately 0.21–1.17 mm. The sandstones are predominantly medium- to fine-grained, with moderate inter-sample variability, indicating fluctuations in sediment supply or hydrodynamic energy during deposition. The standard deviation (σ) has an average of 0.68 and a range of 0.34–1.71, with 17 samples (accounting for 51.5%) having $\sigma < 0.71$, indicating predominantly good to very good sorting. The sorting coefficient averages 1.39, ranging from 1.1655 to 2.9740, and most samples (22 in total, representing 70.9%) have a sorting coefficient < 1.5, which is consistent with the standard deviation results.

These sorting characteristics indicate that the sandstones are generally well sorted, and the concentration of samples within the moderate-to-good sorting range suggests relatively stable, high-energy hydrodynamic conditions during deposition, consistent with traction-current-dominated environments such as fluvial point bars and delta fronts.

Overall, the grain-size characteristics—dominance of medium- to fine-grained sand, good sorting, nearly symmetric grain-size distributions, and moderate concentration—collectively indicate that the Luohe Formation sandstones in the study area were deposited under a stable hydrodynamic regime dominated by traction currents.

The grain-size probability cumulative curves of representative sandstone samples from the upper, middle, and lower members display a typical three-segment pattern, predominantly influenced by saltation and suspension populations. This pattern suggests a strong traction current origin, which is characteristic of fluvial channel deposits (Figure 5).

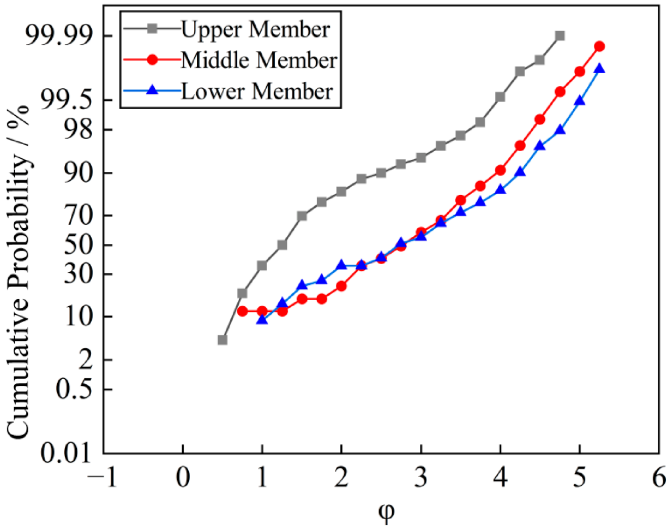


Figure 5. Cumulative curve of particle size probability for representative samples of the Luohe Formation sandstone in Xiaozhuang Coal Mine.

In the Passega C–M diagram [36] (Figure 6), the C value, representing the grain size at the 1% percentile on the cumulative curve, denotes the maximum particle size that could be transported during deposition, thus reflecting the upper limit of hydraulic energy. The M value, corresponding to the 50% percentile, represents the median grain size and indicates the average transport capacity of the depositional current.

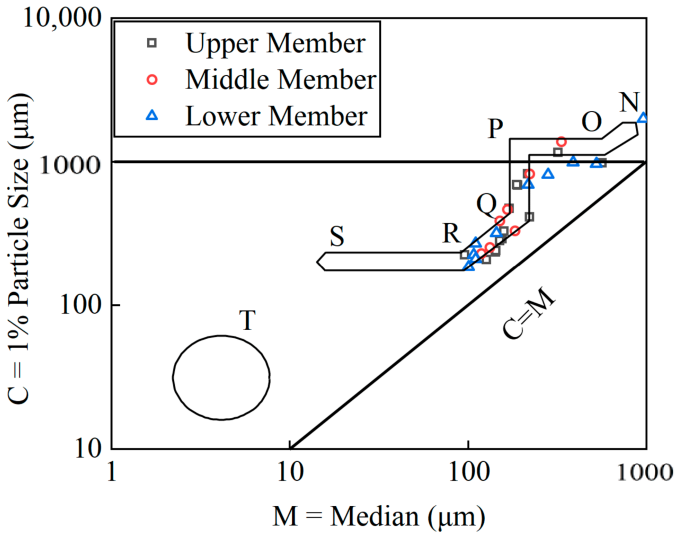


Figure 6. C–M diagram of the Luohe Formation sandstone in Xiaozhuang Coal Mine. C denotes the 1st-percentile grain size (μm) and M denotes the median grain size (μm). Symbols represent the Upper, Middle, and Lower members. The fields NO, OP, PQ, QR, RS, and T correspond to rolling, rolling–suspension, suspension with minor rolling, graded (bottom) suspension, uniform suspension, and pelagic suspension, respectively. This diagram is used to infer transport mechanisms in a hydrodynamic framework and is not intended to uniquely discriminate fluvial versus aeolian depositional settings.

Most samples from the Luohe Formation are plotted within the QR field of the Passega C-M diagram [36], which is indicative of graded suspension transport, while fewer samples are observed in the OP segment (representing rolling and rolling-suspension transport) and the PQ segment (representing suspension and rolling transport). Almost no samples appear in the RS segment, which is associated with uniform suspension. This distribution strongly suggests that sediment transport was dominated by saltation, with only a minor contribution from rolling transport. These characteristics further support the interpretation that the Luohe Formation represents a traction current depositional environment [31] (Figure 6).

Grain-size parameters are widely employed to reconstruct sediment-transport dynamics and to aid facies interpretation. In this study, the quartile deviation–median diameter (QD-Md) discrimination template proposed by Buller and McManus (1974) [37] was used to assist facies discrimination. In this framework, sorting is quantified by quartile deviation (QD) and grain size is represented by median diameter (Md), and facies fields are defined empirically from envelopes derived from sediment datasets. When the (Md, QD) pairs of all samples were projected onto the QD-Md template, most data points were found to fall within, or close to, the fluvial field (Figure 7). Accordingly, the grain-size distribution is interpreted as being consistent with a predominantly fluvial affinity. It should be noted, however, that grain-size–based templates may show overlaps among fields and are not intended to provide a unique environmental diagnosis on their own. When considered together with the C-M distribution and independent sedimentological evidence, the Cretaceous Luohe Formation sandstones in the study area are most plausibly interpreted as fluvial-dominated.

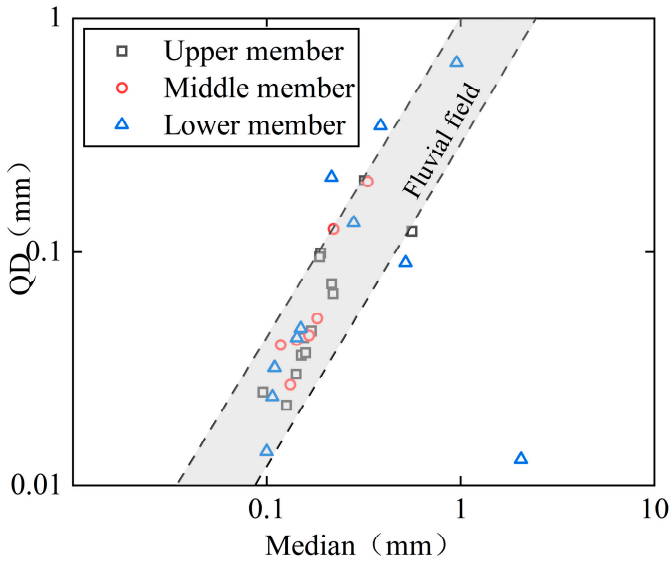


Figure 7. Quartile deviation-median diameter (QD-Md) discrimination template, showing projections of the Luohe Formation sandstone in Xiaozhuang Coal Mine.

3.2.2. Major and Trace Elements Analysis Results

The major element composition of Luohe Formation sandstones is characterized by relatively high SiO_2 and CaO contents, moderate Al_2O_3 levels, and overall depletion of most other oxides compared with average upper continental crust values (Table 1, Figure 8, Normalized values are from the average upper continental crust, with reference values based on chondritic abundances reported by Boynton [38]). This geochemical pattern reflects a quartz-dominated framework composition with variable carbonate cementation and limited chemical alteration of the source rocks.

Table 1. Elemental content (ppm) and characteristic parameters of main, trace and rare earth elements for the Luohe Formation sandstone in Xiaozhuang Coal Mine.

Numbering	SiO_2 (%)	Al_2O_3 (%)	Fe_2O_3 (%)	MgO (%)	CaO (%)	Na_2O (%)	K_2O (%)	MnO (%)	P_2O_5 (%)	TiO_2 (%)	LOI (%)	SUM (%)
XZ01	73.64	9.05	2.66	1.58	3.86	2.2	2.54	0.08	0.06	0.3	3.83	99.80
XZ02	61.38	8.51	3.51	2.87	9.24	1.88	2.26	0.08	0.09	0.44	9.51	99.76
XZ03	62.18	9.52	3.56	2.36	8.64	2.31	2.35	0.08	0.09	0.46	8.24	99.79
XZ04	62.36	9.43	3.76	2.3	8.59	2.3	2.31	0.09	0.09	0.47	8.11	99.81
XZ05	51.67	7.15	2.82	3.13	15.82	1.59	1.83	0.1	0.13	0.44	15.11	99.79
XZ06	58.96	9.18	3.01	1.49	12.08	2.34	2.2	0.09	0.07	0.35	9.99	99.74
XZ07	61.7	10.42	3.97	3.64	6.93	2.28	2.42	0.06	0.09	0.36	7.84	99.73
XZ08	65.37	9.64	3.43	2.37	6.9	2.28	2.34	0.07	0.08	0.37	6.96	99.83
XZ09	71.46	14.3	2.05	1.04	0.64	2.82	5.93	0.07	0.07	0.18	1.23	99.79
XZ10	61.6	9.49	3.86	2.32	8.9	2.27	2.32	0.09	0.11	0.5	8.36	99.82
XZ11	60.58	11.44	5.04	2.44	7.05	2.17	3.08	0.1	0.12	0.57	7.24	99.84
XZ12	69.04	9.55	3.29	1.53	5.72	2.35	2.29	0.07	0.08	0.49	5.45	99.86
XZ13	66.12	9.62	3.59	1.72	6.95	2.35	2.3	0.09	0.08	0.54	6.48	99.84
XZ14	66.35	8.46	2.8	2.09	7.76	1.97	2.37	0.11	0.08	0.43	7.41	99.84
XZ15	72.72	9.1	2.76	1.42	4.4	2.31	2.26	0.05	0.06	0.41	4.34	99.83
XZ16	62.87	9.04	4.1	2.58	7.81	2.06	2.68	0.1	0.09	0.49	8.04	99.85
XZ17	71.15	9.42	3.06	1.61	4.77	2.41	2.49	0.08	0.07	0.35	4.45	99.86
XZ18	69.37	9.14	2.87	1.64	5.99	2.32	2.53	0.08	0.07	0.36	5.48	99.85
XZ19	62.86	9.05	4.33	2.46	7.96	1.89	2.59	0.1	0.09	0.55	7.95	99.83
XZ20	70.59	9.74	3.14	1.82	4.4	2.53	2.78	0.06	0.07	0.4	4.34	99.85
XZ21	72.93	9.18	2.77	1.63	3.99	2.36	2.62	0.06	0.06	0.33	3.95	99.88
XZ22	62.83	9.18	2.62	1.68	9.36	2.59	2.45	0.1	0.06	0.33	8.66	99.86
XZ23	62	9.63	3.04	2.79	8.34	2.22	2.58	0.07	0.11	0.48	8.63	99.88
XZ24	66.66	9.65	1.9	1.98	7.02	2.62	2.45	0.07	0.06	0.31	7.15	99.87
XZ25	59.76	11.02	5.57	3.76	6.28	2.44	3.12	0.07	0.1	0.58	7.15	99.85
XZ26	72.5	8.77	2.5	2.45	3.77	1.96	2.94	0.09	0.06	0.3	4.49	99.83
XZ27	69.18	6.91	2.88	3.04	6.09	1.17	2.42	0.19	0.05	0.25	7.70	99.89
XZ28	71.21	10.18	4.31	3.99	0.88	2.29	2.95	0.05	0.12	0.54	3.33	99.84
XZ29	77.91	8.43	0.9	1.23	2.8	1.9	3.13	0.05	0.04	0.15	3.35	99.89
XZ30	70.17	9.52	3.06	4.5	2.28	1.45	3.46	0.14	0.07	0.35	4.85	99.86
XZ31	78.22	3.24	1.97	2.13	5.65	0.92	0.89	0.1	0.08	0.32	6.39	99.92
XZ32	73.53	7.95	2.21	2.63	3.26	1.38	3.66	0.09	0.07	0.29	4.78	99.84
XZ33	52.52	6	1.68	8.01	11.05	0.9	2.62	0.07	0.08	0.2	16.74	99.87
average	66.41	9.12	3.12	2.49	6.52	2.09	2.64	0.08	0.08	0.39		
Chondrite Meteorite (Boynton)	0.31	0.81	0.12	0.6	0.17	0.07	0.26	0.05	0.32	0.07		

Numbering	B ppm	Li ppm	Sc ppm	V ppm	Cr ppm	Co ppm	Ni ppm	Cu ppm	Rb ppm	Sr ppm	Ba ppm	Hf ppm	Th ppm	U ppm
XZ01	27.8	22.5	7.02	43.7	38.7	6.4	13.2	15.5	75.9	272	776	2.75	5.39	1.52
XZ02	30.4	25.3	8.74	72.1	39.6	7.99	15.4	24.4	67.4	208	869	3.22	8.8	1.55
XZ03	33.6	31.2	10.05	83.5	70	8.86	18.6	19.9	87.4	307	907	3.53	8.88	1.7
XZ04	34.3	27	9.04	67.2	45.2	8.42	16.2	19.7	73.9	261	858	3.75	7.83	1.52
XZ05	36.9	20.5	8.12	58.3	44.6	6.69	14.4	13.2	60.8	198	621	4.42	7.97	1.5
XZ06	29.6	20.4	8.85	53.3	44.1	6.74	13.6	13.9	77.4	343	1818	2.8	6.67	1.31
XZ07	54.5	35.3	8.46	60.3	40.9	9.84	18.5	19.6	74.6	270	667	2.31	6.98	1.77
XZ08	36.1	26.4	7.72	61.6	42.1	8.08	16.5	16.7	71.7	264	853	2.7	6.81	1.58
XZ09	40.4	15.4	8.37	18.4	22.6	2.96	6.64	8.45	217	138	1425	3.63	11.3	0.89
XZ10	43.7	29.1	10.02	69.4	54.5	8.83	18.2	17.4	82.4	275	684	4.38	9.24	1.75
XZ11	52.5	48.6	12.73	98.1	69.8	13.5	29	23.9	113	187	897	3.46	9.04	1.47
XZ12	34.7	24.7	8.6	59.4	39.5	8.06	14.5	17.4	68.6	248	726	2.79	6.52	1.71
XZ13	38.6	25.5	10.46	71.9	45.4	8.41	15.1	16.2	72.2	288	671	5.4	8.73	2.18
XZ14	37.8	26.2	8.88	65	48.7	7.73	17	20.9	80	258	804	3.27	9.09	1.24
XZ15	44.4	22.5	7.59	50.4	33.3	6.67	12.5	15.5	69.9	262	731	2.25	5.22	1.68
XZ16	32.2	26.9	8.74	73.1	60.3	9.44	16.8	15.3	82.3	237	806	3.96	10.1	2.12

Table 1. *Cont.*

Numbering	B ppm	Li ppm	Sc ppm	V ppm	Cr ppm	Co ppm	Ni ppm	Cu ppm	Rb ppm	Sr ppm	Ba ppm	Hf ppm	Th ppm	U ppm
XZ17	33.3	27.9	8.25	52	43.7	7.29	14.8	16.2	78.9	265	814	2.6	5.78	1.85
XZ18	38.3	27.9	8.44	51.1	38	7.73	14.6	16.5	77.5	261	811	2.58	5.87	1.68
XZ19	35.5	27.8	9.1	76.8	48.6	9.15	18.4	17.3	79.8	233	895	3.76	8.17	2.26
XZ20	33.3	24.2	9.3	54.5	37.1	7.7	15.2	13.9	86.8	255	794	3.39	7.47	1.9
XZ21	31.7	21	7.28	44.4	28.8	6.33	11.9	13.5	73.7	248	730	2.6	5.55	1.46
XZ22	26.9	24.1	9.24	42	39.8	7.59	15.8	18.6	76.1	232	753	2.37	5.8	2.08
XZ23	32.8	41.7	10.5	65.3	53.9	11.9	25.2	32.9	96.8	164	646	3.53	7.12	2.37
XZ24	29.8	27.2	8.38	44.4	38.8	7.37	14.7	36.7	72.6	202	777	2.36	5.06	1.47
XZ25	32.2	55.2	12.36	90.6	62.4	13.8	28.3	17.5	114	183	736	3.62	8.58	2.97
XZ26	27.6	35.4	6.46	41.2	34.5	5.44	11.7	10.1	90.2	190	1051	3.37	5.87	1.87
XZ27	30.9	31.1	5.35	37.4	31	5.26	13.1	13	81.4	136	576	2.2	5.32	1.44
XZ28	42.3	75.9	10.72	67.9	57.3	8.36	16.9	10.1	97.3	176	685	7.72	11.3	3.04
XZ29	25.9	35.1	4.21	23.9	17.2	2.87	6.28	15	96.1	151	652	1.63	4.68	1.46
XZ30	40.8	61.4	6.7	39	44.6	7.38	15	9.54	113	178	834	2.35	7	1.67
XZ31	19.9	17.6	4.42	19.6	21.5	3.55	6.36	6.79	27	95.3	305	1.96	3.54	1.56
XZ32	26.2	31.4	4.66	34.7	28.8	4.33	9.27	6.4	130	147	876	4.11	10.1	2
XZ33	20.6	22.9	4.62	27.9	25.4	3.82	10.3	6.22	87.5	185	690	1.87	5.72	1.4
Chondrite Meteorite (Boynton)	0.21	0.03	0.21	0.03										

Numbering	La ppm	Ce ppm	Pr ppm	Nd ppm	Sm ppm	Eu ppm	Gd ppm	Tb ppm	Dy ppm	Ho ppm	Er ppm	Tm ppm	Yb ppm	Lu ppm
XZ01	24.9	44	4.89	16.3	3.03	0.88	2.74	0.42	2.13	0.46	1.24	0.19	1.35	0.21
XZ02	32.2	60.4	6.6	22.7	4.1	0.99	3.82	0.52	2.7	0.54	1.59	0.23	1.61	0.25
XZ03	39.6	75	8.27	26.7	5.18	1.26	4.57	0.72	3.64	0.72	2.02	0.29	2.02	0.31
XZ04	30.9	55.9	6.37	21.6	4.34	1.01	3.46	0.57	2.94	0.58	1.62	0.23	1.75	0.27
XZ05	30	51.3	6.36	22.2	4.37	1.02	4.06	0.69	3.79	0.79	2.1	0.3	2.09	0.32
XZ06	22.8	41.3	4.94	16.7	3.32	1.08	3.02	0.5	2.61	0.55	1.53	0.23	1.69	0.27
XZ07	28.5	53	5.83	20.6	4.18	1.02	3.63	0.59	3.08	0.64	1.74	0.25	1.68	0.25
XZ08	35.8	71.8	7.74	24.7	4.69	1.24	4.16	0.64	3.45	0.7	1.89	0.26	1.81	0.26
XZ09	35.9	78.9	8.48	27.6	5.16	1.11	4.37	0.73	4.05	0.85	2.45	0.37	2.51	0.37
XZ10	33.7	62	6.97	24.8	4.68	1.13	4.05	0.6	3.1	0.62	1.75	0.25	1.88	0.29
XZ11	31.4	61.2	6.84	22.7	4.63	1.28	4.54	0.72	3.74	0.74	2.03	0.28	2.06	0.32
XZ12	25.7	48.1	5.74	19	3.71	0.98	3.3	0.51	2.72	0.56	1.5	0.24	1.62	0.25
XZ13	31	57.7	6.64	21.7	4.28	1.08	3.7	0.55	2.84	0.61	1.69	0.25	1.77	0.28
XZ14	35	70.8	7.5	23.3	4.32	1.12	4.04	0.55	2.87	0.56	1.73	0.25	1.72	0.26
XZ15	20.7	39.6	4.63	15.2	2.94	0.89	2.57	0.39	2.15	0.42	1.16	0.18	1.15	0.18
XZ16	41.9	79.7	8.27	26.1	4.63	1.07	4.05	0.61	3.09	0.6	1.72	0.25	1.89	0.27
XZ17	22.9	42.8	4.9	16.3	3.16	0.85	2.87	0.43	2.29	0.45	1.31	0.19	1.29	0.21
XZ18	21.4	41.1	4.77	16.8	3.34	0.91	2.8	0.48	2.51	0.48	1.39	0.2	1.4	0.22
XZ19	33.8	60.7	6.65	21.9	4.06	1.08	3.56	0.55	2.85	0.56	1.64	0.25	1.79	0.27
XZ20	29.2	52.1	5.42	18.1	3.45	0.96	3.25	0.47	2.5	0.5	1.45	0.21	1.5	0.23
XZ21	24.2	44	4.81	15.9	3.06	0.9	2.92	0.41	2.19	0.44	1.27	0.18	1.34	0.2
XZ22	27.1	46.8	5.76	19.6	3.93	1.07	3.55	0.51	2.65	0.53	1.52	0.22	1.58	0.24
XZ23	23	41.3	5.2	17.3	3.6	0.91	3.47	0.55	3.11	0.65	1.83	0.28	1.97	0.29
XZ24	18.9	38.1	4.4	14.5	2.82	0.81	2.73	0.41	2.16	0.44	1.2	0.18	1.32	0.19
XZ25	32.3	59.3	6.5	21.3	4.13	0.98	3.88	0.56	3	0.58	1.72	0.25	1.7	0.26
XZ26	18.3	36.8	3.89	13.7	2.68	0.79	2.53	0.38	2.09	0.42	1.24	0.19	1.32	0.2
XZ27	21.7	41	4.6	16.7	3.24	0.85	3.13	0.49	2.47	0.49	1.37	0.19	1.37	0.21
XZ28	26.4	52.1	5.95	19.7	3.77	0.87	3.33	0.49	2.52	0.53	1.63	0.25	1.87	0.28
XZ29	15.5	32.8	3.53	12.2	2.37	0.67	2.18	0.32	1.65	0.31	0.85	0.12	0.93	0.14
XZ30	19.8	38	4.34	14.8	2.96	0.78	2.81	0.44	2.6	0.51	1.38	0.19	1.43	0.2
XZ31	22	34.9	4.14	14.3	2.74	0.56	2.64	0.41	2.12	0.41	1.12	0.15	1.09	0.16
XZ32	29.1	53.3	6.14	20.3	3.78	0.86	3.41	0.54	2.73	0.52	1.58	0.23	1.66	0.24
XZ33	17.9	36.1	4.19	14.3	2.82	0.61	2.43	0.4	2.03	0.41	1.19	0.17	1.23	0.18

Table 1. *Cont.*

Numbering	La/Th ppm	La/Sc ppm	Co/Th ppm	∑REE ppm	∑LREE ppm	∑HREE ppm
XZ01	4.62	3.55	1.19	102.74	94.01	8.73
XZ02	3.66	3.68	0.91	138.29	127.03	11.26
XZ03	4.46	3.94	1	170.25	155.97	14.29
XZ04	3.94	3.41	1.08	131.51	120.08	11.43
XZ05	3.77	3.7	0.84	129.44	115.31	14.13
XZ06	3.41	2.57	1.01	100.49	90.09	10.41
XZ07	4.09	3.37	1.41	124.99	113.14	11.85
XZ08	5.26	4.64	1.19	159.23	146.07	13.16
XZ09	3.18	4.29	0.26	172.8	157.1	15.7
XZ10	3.65	3.37	0.96	145.89	133.35	12.54
XZ11	3.47	2.47	1.49	142.55	128.09	14.45
XZ12	3.94	2.99	1.24	113.85	103.14	10.7
XZ13	3.55	2.96	0.96	134.07	122.39	11.69
XZ14	3.84	3.94	0.85	153.99	142.01	11.98
XZ15	3.96	2.72	1.28	92.09	83.89	8.2
XZ16	4.16	4.8	0.94	174.19	161.72	12.48
XZ17	3.96	2.78	1.26	99.9	90.85	9.05
XZ18	3.66	2.54	1.32	97.8	88.33	9.48
XZ19	4.14	3.72	1.12	139.71	128.25	11.46
XZ20	3.91	3.14	1.03	119.41	109.32	10.1
XZ21	4.36	3.33	1.14	101.73	92.78	8.95
XZ22	4.68	2.93	1.31	115.07	104.28	10.79
XZ23	3.24	2.2	1.67	103.47	91.33	12.15
XZ24	3.73	2.25	1.46	88.14	79.51	8.63
XZ25	3.76	2.61	1.61	136.37	124.42	11.95
XZ26	3.11	2.83	0.93	84.48	76.11	8.37
XZ27	4.09	4.06	0.99	97.86	88.14	9.72
XZ28	2.35	2.47	0.74	119.66	108.76	10.9
XZ29	3.31	3.67	0.61	73.54	67.03	6.51
XZ30	2.82	2.95	1.05	90.17	80.6	9.57
XZ31	6.21	4.97	1	86.7	78.6	8.1
XZ32	2.87	6.23	0.43	124.31	113.4	10.91
XZ33	3.13	3.88	0.67	83.94	75.9	8.04

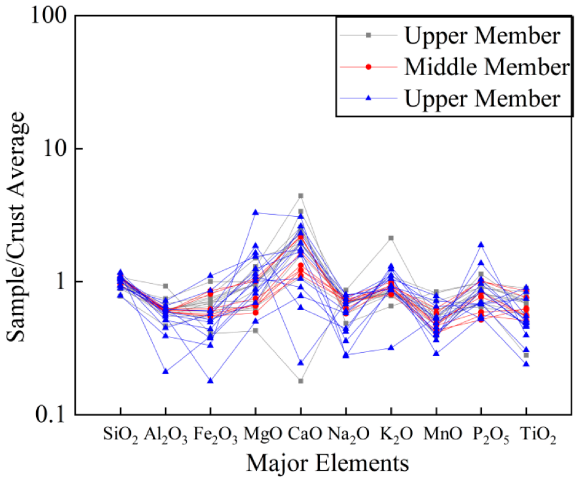


Figure 8. Upper continental crust-normalized multi-element distribution patterns for the Luohe Formation sandstone in Xiaozhuang Coal Mine.

SiO_2 contents show a wide range (51.67–78.22 wt.%, average 66.41 wt.%), consistent with petrographic observations indicating quartz as the dominant detrital mineral. The relatively moderate Al_2O_3 content (average 9.12 wt.%) suggests a subordinate contribution from aluminosilicate minerals such as feldspar, mica, and clay minerals, implying an overall

moderate compositional maturity of the sandstones. CaO exhibits pronounced enrichment and strong variability (0.64–15.82 wt.%, average 6.52 wt.%), indicating heterogeneous distribution of carbonate components within the reservoir. In contrast, Fe_2O_3, MgO, Na_2O, K_2O, MnO, P_2O_5, and TiO_2 are generally depleted relative to average crustal values, suggesting limited input from ferromagnesian minerals and minimal enrichment of heavy minerals. The Na_2O/K_2O ratios further indicate relatively low feldspar alteration, consistent with weak chemical weathering conditions in the source area.

The trace-element analytical results for all 33 samples of the Luohe Formation sandstones are shown in Table 1. The analysis indicates that elements such as B, Li, Rb, and Ba exhibit enrichment, while the remaining elements show varying degrees of depletion (Figure 9, Normalized values are from the average upper continental crust, with chondritic reference data after Boynton [38]).

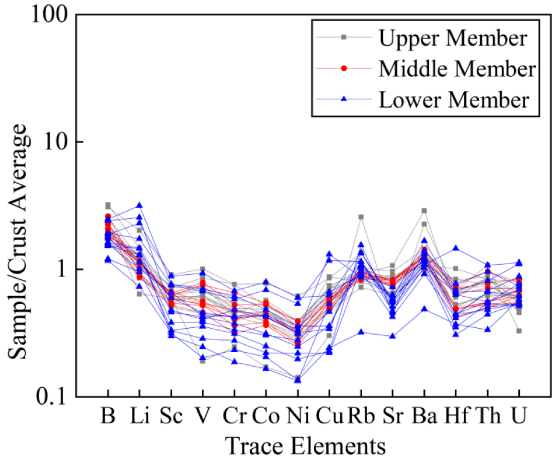


Figure 9. Upper continental crust-normalized trace element distribution patterns for the Luohe Formation sandstone in Xiaozhuang Coal Mine.

The rare earth element (REE) data of all 33 samples were normalized using chondrite values recommended by Boynton (1984) [38]. The resulting REE distribution patterns are illustrated in Figure 10 (Potential provenance fields are shown for comparison. Normalization values are from Boynton [38]; shaded provenance fields are compiled from published data [15]). The patterns display a marked enrichment in light rare earth elements (LREE), depletion in heavy rare earth elements (HREE), and a slight negative europium anomaly. Overall, the REE patterns show a rightward (or right-inclined) trend [39].

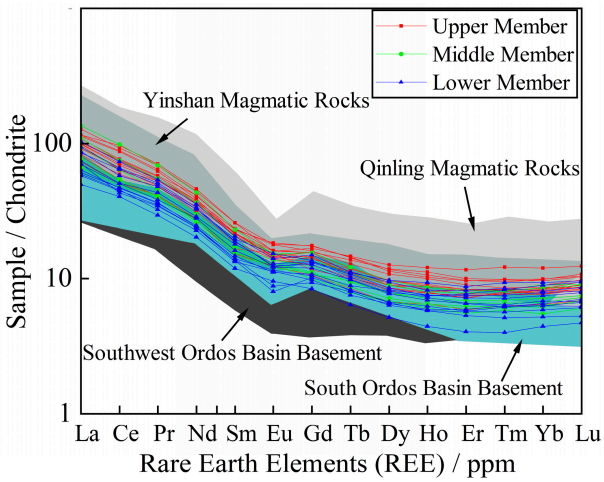


Figure 10. Chondrite-normalized rare earth element (REE) distribution patterns for the Luohe Formation sandstone in Xiaozhuang Coal Mine.

4. Tectonic Setting of the Provenance Area and Provenance Analysis

4.1. Framework Mineral Composition

Petrographic observations are presented to evaluate the extent to which the sandstones preserve primary depositional signatures (Figures 3 and 4). The Luohe Formation sandstones in the study area include coarse-, medium-, and fine-grained varieties, yet their framework compositions are broadly similar and dominated by quartz, with subordinate feldspar and minor biotite. Cement content is low and cementation is generally weak, whereas primary intergranular pores are commonly preserved, with only minor pore occlusion by thin, late-stage clay coatings. These features indicate that the samples have experienced relatively minor late-stage diagenetic alteration; therefore, their bulk mineralogical and geochemical compositions can be considered representative of depositional conditions, thus providing a sound basis for subsequent provenance and paleoenvironmental interpretations.

4.2. Tectonic Setting of the Source Area

Geochemical methods are among the most essential techniques for reconstructing sedimentary processes, particularly for provenance tracing and tectonic–sedimentary setting analysis of clastic rocks [40,41]. Variations in the compositions of major elements can provide constraints on the tectonic-sedimentary setting during diagenesis. In contrast, trace elements and rare earth elements (REEs), owing to their relative immobility, serve as reliable indicators of provenance characteristics. These elements are crucial for determining the tectonic background, provenance rock nature, and depositional environment.

The K_2O/Na_2O–SiO_2 diagram (Figure 11, Discrimination diagrams proposed by Roser, B.P. & Korsch, R.J. [22]), frequently employed to infer provenance area tectonics for sandstones and mudstones, reveals that the majority of samples from the Luohe Formation in the study area are situated within the active continental margin field. In contrast, samples from the lower part of the formation are positioned within the passive continental margin field. This suggests a mixed provenance, with a dominance of input from active continental provenances, supplemented by material from passive continental provenances.

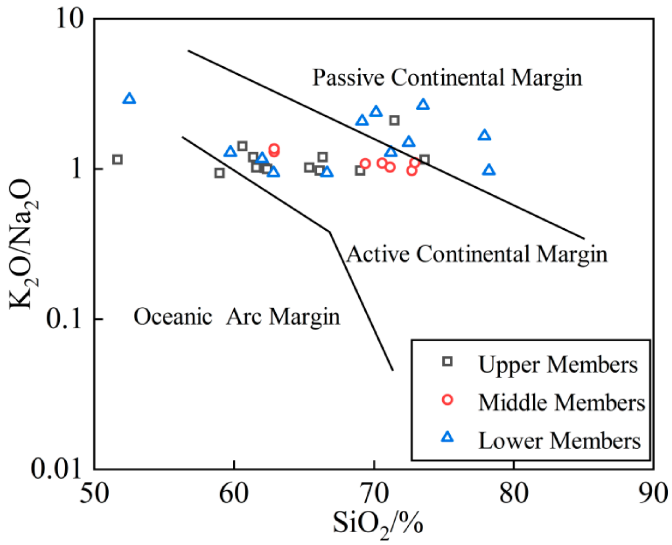


Figure 11. K_2O/Na_2O vs. SiO_2 diagram for samples of the Luohe Formation sandstone in Xiaozhuang Coal Mine.

The aeolian sandstones, composed mainly of quartz and feldspar, are characterized by high maturity, with their provenance corresponding to a passive continental margin background [10]. Based on a comprehensive study of the geochemical characteristics of the

Xiaozhuang study area, major element discrimination diagrams indicate that most of the provenance corresponds to an active continental margin, with only some samples from the lower member of the Luohe Formation plotting in the field of passive continental margin. Combined with grain-size analysis, most samples fall within the QR segment (representing traction current deposits) on the C-M plot. This finding aligns with previous studies that interpret the strata in the study area as fluvial sandstones.

Tectonic discrimination diagrams as proposed by Bhatia and Crook [41] for sandstones and mudstones, including the Ti/Zr–La/Sc, La–Th–Sc, and Th–Sc–Zr/10 plots (Figure 12), were used to analyze the trace element data from sandstone samples of the Luohe Formation in Xiaozhuang Coal Mine. The majority of the samples plot within the fields of active continental margin and continental island arc. When combined with the major and trace element discrimination diagrams, these results suggest that the provenance tectonic setting is primarily associated with an active continental margin, with notable influence from a continental island arc.

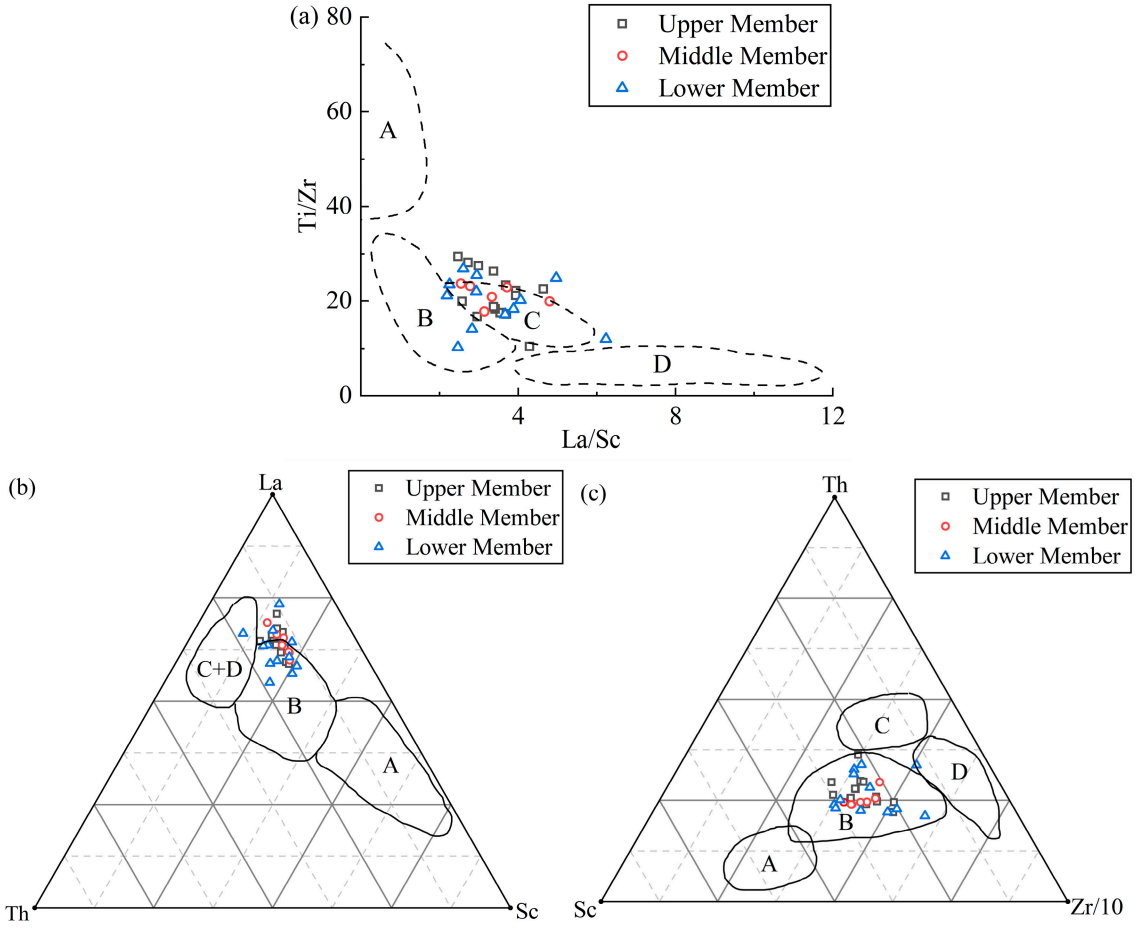


Figure 12. Diagrams for samples of the Luohe Formation sandstone in Xiaozhuang Coal Mine. (**a**) Ti/Zr-La/Sc; (**b**) La-Th-Sc; and (**c**) Th-Sc-Zr/10. A—Oceanic island arcs; B—Continental island arcs; C—Active continental margins; D—Passive continental margins.

4.3. Provenance Analysis

Provenance analysis is a key approach for reconstructing the evolutionary history of sedimentary basins and associated paleoenvironmental conditions. Previous studies have indicated that the sedimentary provenance of the Ordos Basin is predominantly derived from multiple source regions: the Yinshan Mountains to the north, the Daqingshan Uplift to the northeast, the ancient "Gulüliang" highland to the west, the Qinling orogenic belt to the south, the Alxa Block to the northwest, and the eastern Qilian orogenic belt to the

southwest [6]. Sedimentary rocks originating from the same source area typically exhibit highly comparable rare earth element (REE) distribution patterns. Thus, comparing REE distribution patterns between samples from the study area and those from potential source terranes provides a robust approach for provenance identification.

Rare earth element (REE) distribution patterns of Luohe Formation sandstone samples from the Xiaozhuang Coal Mine (Figure 12) exhibit distinct vertical variations, particularly in the lower interval (301–436 m). Here, the REE patterns closely resemble those of the southern Ordos Basin basement, indicating a dominant provenance contribution from the southern basement. In the middle member (231–301 m), the REE patterns show greater dispersion, overlapping with both the Qinling magmatic rocks and southern Ordos Basin basement fields—suggesting a mixed provenance derived from these two sources. In the upper member (116–231 m), the REE patterns predominantly fall within the field of Qinling magmatic rocks, reflecting a complete shift in sediment source to the northern Qinling magmatic arc.

The Xiaozhuang area, situated at the southwestern margin of the Ordos Basin—a tectonically complex zone where multiple terranes converge—likely received detritus from several adjacent regions, including the Northern Qilian Orogen, the Northern Qinling Orogen, the Alxa Block, and the northern margin of the North China Craton. Overall, the early-stage provenance of the Luohe Formation was primarily associated with the southern basement of the Ordos Basin. However, with progressive tectonic uplift and structural evolution, sediment sources underwent gradual shifts and mixing, ultimately becoming dominated by material input from the Qinling magmatic belt.

To further identify the source rock types, discrimination diagrams such as Co/Th–La/Sc [42] and La/Th–Hf [43] were utilized for systematic geochemical analysis. In the Co/Th–La/Sc diagram (Figure 13a), most sample points plot adjacent to the Felsic rock region, including adjacent rhyolite and granite, within the area between rhyolite and granite fields. An elevated La/Sc ratio indicates contributions from felsic components, whereas a higher Co/Th ratio reflects input from intermediate to mafic components. In the La/Th–Hf diagram (Figure 13b), the majority of Luohe Formation samples cluster within the felsic to mafic igneous rock provenance fields. Combined with tectonic discrimination results (e.g., continental island arc setting), findings from both diagrams strongly indicate that Luohe Formation sandstones were primarily derived from a mixture of felsic and mafic igneous source rocks.

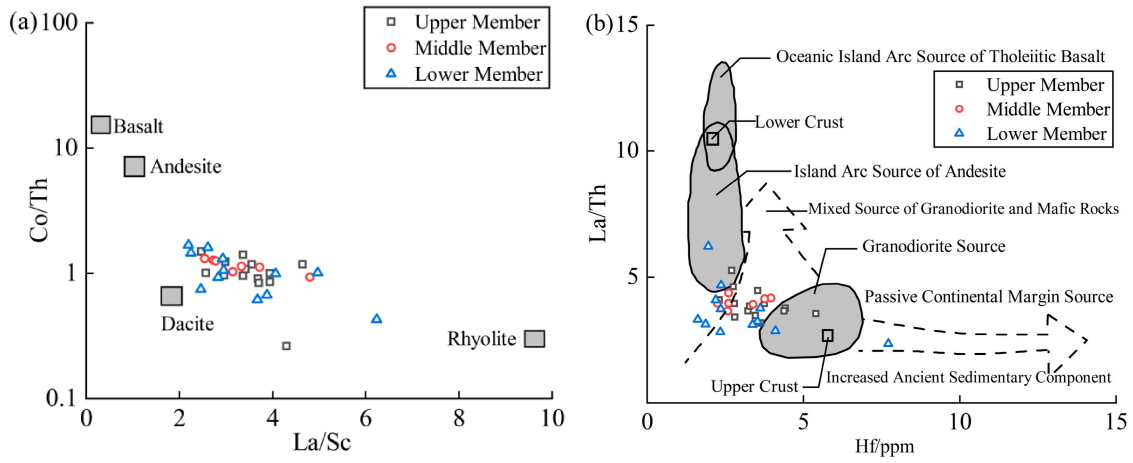


Figure 13. Provenance rock identification diagram for the Luohe Formation sandstone in Xiaozhuang Coal Mine. (**a**) Co/Th–La/Sc diagram; (**b**) La/Th–Hf diagram.

The characteristics of framework grains of the Luohe Formation in the Xiaozhuang Coal Mine also indicate a mixed provenance. The sandstones show low compositional maturity, with low quartz content (30–51%) and relatively high feldspar (9–20%) and lithic fragments (10–22%). Meanwhile, plagioclase dominates the feldspar, indicating a source of intermediate-mafic magmatic rocks, volcanic rocks, and metamorphic rocks. The lithic fragments are mainly magmatic and metamorphic, with very low sedimentary rock fragments. The diverse types of lithic fragments also suggest a mixed provenance.

5. Sedimentary Environment Analysis

5.1. Paleo-Climate

Climate conditions exert a significant influence on the trace element ratios in sediments. The Sr/Cu ratio—where strontium (Sr) tends to enrich under arid conditions and copper (Cu) under humid conditions—is widely used as a paleoclimate proxy [44]. Sr/Cu ratios between 1.3 and 5.0 indicate warm and humid climates, whereas ratios > 5.0 suggest hot and arid conditions. In the Luohe Formation sandstones from the Xiaozhuang Coal Mine (Binchang Mining Area), Sr/Cu ratios range from 4.98 to 29.8, with a mean of 15.11, indicating predominantly hot and arid climatic conditions during sedimentation (Figure 14).

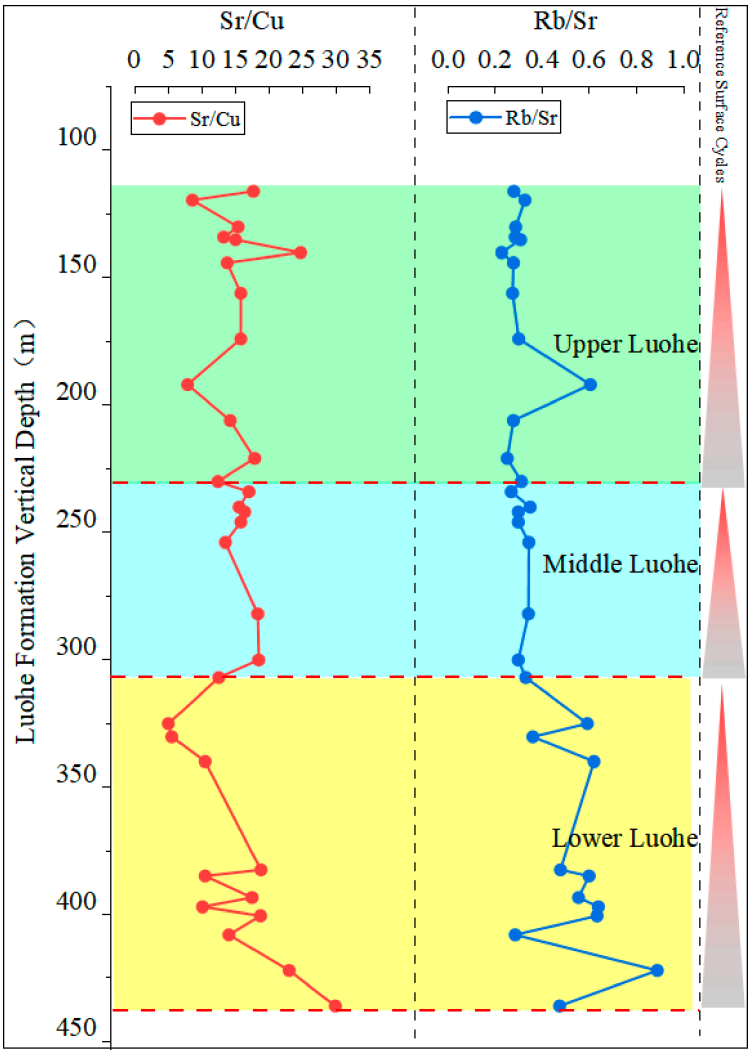


Figure 14. Vertical changes in Sr/Cu, Rb/Sr of the Luohe Formation sandstone in Xiaozhuang Coal Mine.

Additionally, the Rb/Sr ratio serves as a sensitive indicator of climatic change [45]. Rb is relatively stable and less susceptible to environmental changes, whereas Sr is more easily leached. Consequently, low Rb/Sr ratios reflect arid conditions, whereas high ratios indicate humid environments. The Rb/Sr ratios in the study area range from 0.22 to 1.57, with a mean of 0.43, further supporting an arid depositional setting for the Luohe Formation.

The Sr/Cu and Rb/Sr ratios show no significant correlation, likely due to the limited variability in Rb content; the Rb/Sr ratios are generally clustered around 0.4 within a narrow range. The consistently low Rb/Sr ratios further corroborate that the Luohe Formation was deposited under predominantly arid climatic conditions.

5.2. Paleo-Salinity

To comprehensively evaluate the paleosalinity of the Luohe Formation sandstones in Xiaozhuang Coal Mine, four geochemical proxies were employed: boron (B), strontium (Sr), lithium (Li), and nickel (Ni). According to Degens et al. [46], these elements occur within the rock grain framework via isomorphous substitution or metasomatic replacement and are less affected by diagenetic processes [47–49]. B concentration serves as a valuable indicator for distinguishing between marine and freshwater depositional environments. When B < 80 ppm, the environment is interpreted as freshwater; values between 80–120 ppm indicate a transitional (brackish or marginal marine) setting; and values exceeding 120 ppm are considered indicative of a saline (marine) environment. However, boron (B) generally occurs in the form of phyllosilicates, particularly mica, serpentine, and montmorillonite, and may be subject to only limited effects induced by diagenetic processes. Using it as a paleosalinity reference indicator can also improve its generalizability. Previous studies have demonstrated that Li concentrations exceeding 150 ppm and Ni concentrations greater than 40 ppm are characteristic of saline or marine depositional settings. Conversely, Li < 90 ppm and Ni between 20–25 ppm are typically associated with freshwater (continental) environments [43].

The concentration ranges of B, Sr, Li, and Ni in the Luohe Formation sandstones are primarily within the values defined for freshwater continental environments (see Table 2). Based on the trace element proxies for paleosalinity and the results of grain size analysis, it can be concluded that the sedimentary environment of the sandstones of the Luohe Formation in Xiaozhuang Coal Mine, Binchang Mining Area, was fluvial.

Table 2. Paleosalinity trace element discriminators.

Trace Elements	Brine (Marine Facies)	Brackish Water (Transitional Marine-Terrestrial Facies)	Freshwater (Terrestrial Facies)	Luohe Formation Sandstone Samples	
				Range of Variation	Average Value
B	>120	80–120	<80	19.89–54.47	34.40
Sr	800~1000	500–800	100~500	95.27–343.33	221.79
Li	>150	90–150	<90	15.40–75.94	30.76
Ni	>40	25–40	<25	6.27–28.96	15.27

Note: The units for elements B, Sr, Li, and Ni are ppm.

5.3. Oxidation-Reduction Conditions

In the identification and analysis of ancient sedimentary environments, the relative concentration ratios of redox-sensitive elements in sediments play a crucial role. Jones [50] proposed that the ratios of U/Th, V/Cr, and Ni/Co serve as reliable proxies for determining the redox conditions of water bodies. Similar to the elements discussed in Section 5.2, U and Th are predominantly hosted in zircon, whereas V, Cr, Ni, and Co are concentrated in magnetite [50,51]. Specifically, the geochemical behaviors of U (uranium) and Th (thorium) exhibit significant differences under varying depositional conditions: U has a low solubility in reducing environments and tends to remain in situ. In contrast, under oxidative

conditions, U is readily oxidized and migrates. In contrast, Th behaves differently, as its solubility remains low in various sedimentary environments, making it more likely to be enriched in sediments.

Furthermore, the mobility of Ni (nickel) is significantly influenced by the redox state of the depositional environment, exhibiting migration in oxidizing conditions and precipitation under reducing conditions. Importantly, Co (cobalt) is more sensitive to redox reactions in reducing environments than Ni, leading to a more pronounced depletion of Co in reduced sediments and consequently a higher Ni/Co ratio relative to other conditions [50]. This variation provides important chemical indicators for identifying ancient sedimentary environments.

As a reducing element, V (vanadium) serves as an indicator of the environmental redox state. In addition to the V/Cr ratio, Kimura and Watanabe [52] argue that the V/Sc ratio—using Sc (scandium), which shares similar insolubility in reducing states with V—can be a more effective and accurate indicator of V enrichment. A lower V/Cr vs. V/Sc ratio indicates a more oxidizing environment. In the Luohe Formation samples from Xiaozhuang Coal Mine, the variations of the U/Th, V/Cr, Ni/Co, and V/Sc ratios all fall within the ranges corresponding to oxidizing environments (see Table 3). As shown in Figure 15, the data points for the samples are concentrated in the oxidizing environment zone, indicating that the sedimentary processes in all three members of the Luohe Formation were characterized by strong oxidation.

Table 3. Discrimination of Ancient Redox Conditions.

Trace Elements	Reducing Environment	Weak Oxidation—Weak Reduction Environment	Oxidizing Environment	Sample Data Statistics	
				Range of Values	Average Value
U/Th	>1.25	0.75–1.25	<0.75	0.07–0.44	0.25
Ni/Co	>7	5–7	<5	1.77–2.69	2.04
V/Cr	>4.5	2.0–4.25	<2	0.81–1.81	1.29
V/Sc	>140	60–140	<60	2.20–8.44	6.57

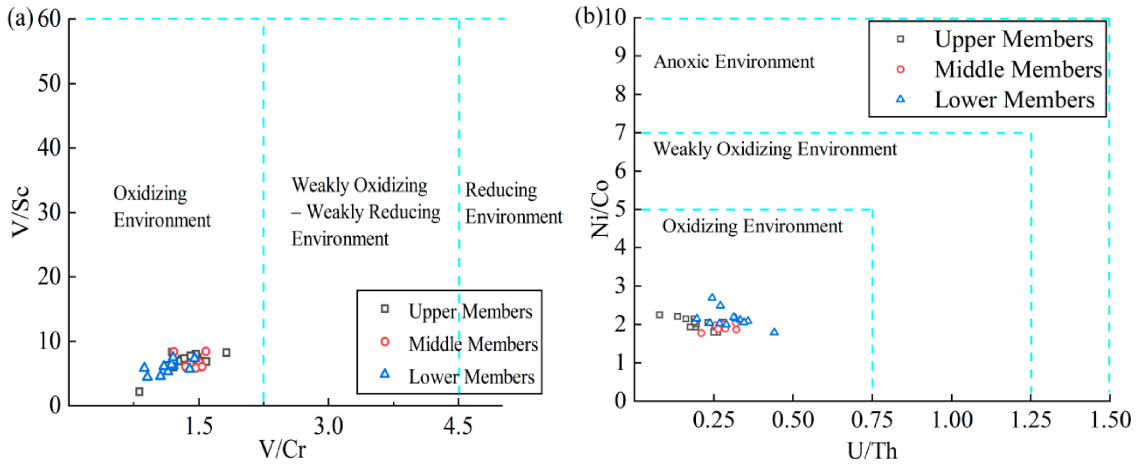


Figure 15. Discrimination diagrams for redox conditions of the Luohe Formation sandstone in Xiaozhuang Coal Mine. (**a**) V/Cr vs. V/Sc and (**b**) U/Th vs. Ni/Co.

6. Conclusions

The Lower Cretaceous Luohe Formation in the Xiaozhuang Coal Mine is for the first time subdivided into three lithologic members, documenting a complete depositional energy cycle from high energy to low energy and back to higher energy conditions. Provenance analysis newly identified an upward shift from dominant basement materials of the

North China Craton to a mixed source increasingly influenced by magmatic rocks of the Northern Qinling Belt. Integrated sedimentological and geochemical data demonstrate that the Luohe Formation was deposited in an overall hot, arid, freshwater, and highly oxidizing fluvial system. Despite short-term climatic fluctuations in the lower and upper members, the entire succession represents a persistent continental depositional setting, providing new constraints on the paleoenvironmental evolution of the region.

Author Contributions: All authors contributed to the study conception and design. S.L., Y.C., and S.W. wrote the main manuscript. L.H. and X.G. analyzed the data. G.L. and L.Y. prepared figures. All authors have read and agreed to the published version of the manuscript.

Funding: This paper is funded by the Key Program of the National Natural Science Foundation of China (42330808) and the Major Science and Technology Special Project of Shaanxi Coalfield Geology Group Co., Ltd. (SMDZ-2023ZD-5), and supported by the State Key Laboratory of Geological Support for Coal Green Development, Xi'an University of Science and Technology and Key Laboratory of Coal Resources Exploration and Comprehensive Utilization, Ministry of Natural Resources, Xi'an. The views expressed are the authors' alone.

Data Availability Statement: All data generated or analyzed during this study are included in this published article.

Acknowledgments: During the preparation of this work, the authors used ChatGPT 5 in order to improve the language used. After using this tool, the authors reviewed and edited the content as needed and take full responsibility for the content of the publication.

Conflicts of Interest: Liangliang He (L.H.), Xiang Guo (X.G.), Guijuan Li (G.L.), and Lei Yang (L.Y.) are employed by 186 Coalfield Geological Co., Ltd. The remaining authors (Yue Cai, Shiwu Liu, and Shaoni Wei) declare that they have no known competing financial interests or personal relationships that could have appeared to influence the work reported in this paper. All authors confirm that the research was conducted in the absence of any commercial or financial relationships that could be construed as a potential conflict of interest.

References

1. Wang, S.M. Ordos basin tectonic evolution and structural control of coal. *Geol. Bull. China* **2011**, *30*, 544–552. [CrossRef]
2. Zhang, Z.Y. Sedimentary Characteristics of the Cretaceous Luohe Formation–Huanhe Huachi Formation in the Ordos Basin. Master's Thesis, Chang'an University, Xi'an, China, 2005. Available online: https://m.book118.com/html/2019/0630/8071123115002032.shtm (accessed on 14 January 2026).
3. Dong, S.N.; Fan, M.; Guo, X.M.; Liu, Y.F.; Guo, K.; Ji, Z.K.; Li, C.F.; Xue, X.Y. Characteristics of Typical Flood Hazards and Management Techniques in Coal Mines in Shaanxi Province. *J. China Coal Soc.* **2024**, *49*, 902–916. [CrossRef]
4. Li, C.F.; Liu, Y.X.; Zhang, J.K.; Ren, D.; Hou, T.; Liu, Z.; Xu, X.; Ma, J.; Wang, Q.; Duan, X.; et al. Study on Vertical Variability of Hydrogeological Characteristics of Luohe Formation Based on Double Packer Pumping Test. *Coal Geol. Explor.* **2023**, *51*, 55–64. [CrossRef]
5. Guo, X.M. Sedimentary Control on Groundwater in Luohe Formation and Water Flow Field Response Regularity After Mining Disturbance in Binchang Mining Area. Ph.D. Thesis, The China Coal Research Institute, Beijing, China, 2022. [CrossRef]
6. Xie, Y.; Wang, J.; Jiang, X.S.; Li, M.H.; Xie, Z.W.; Luo, J.N.; Hou, G.C.; Liu, F.; Wang, Y.H.; Zhang, M.S.; et al. Sedimentary Characteristics of the Cretaceous Desert Facies in the Ordos Basin and Its Hydrogeological Significance. *Acta Sedimentol. Sin.* **2005**, *23*, 73–83. [CrossRef]
7. Li, X.L. Sedimentary Environment and Microscopic Water Control Law of Luohe Formation in Gaojiapu Coal Mine, Binchang Mining Area. *Coal Geol. Explor.* **2025**, *53*, 12. [CrossRef]
8. Zhu, Q.; Si, Q.H.; Li, J.G.; Miao, P.S.; Wen, S.B.; Li, G.Y.; Zhang, B. Two Genetic Types of Gray Sandstone in Lower Cretaceous Luohe Formation in Southwestern Ordos Basin and Their Uranium-Bearing Property. *Earth Sci.* **2023**, *48*, 3995–4016. [CrossRef]
9. Jin, R.S.; Zhu, Q. Supernormal Enrichment Mechanism and Metallogenic Process of Sandstone-Type Uranium Deposit in Aeolian Sedimentary System of Jingchuan Area, Ordos Basin. *Acta Geol. Sin.* **2023**, *97*, 725–737. [CrossRef]
10. Zhu, X.R.; Liu, L.; Jia, S.K.; Li, R.Q.; Gong, Y.D. Geochemistry and Provenance Characteristics of Aeolian Sandstones of the Cretaceous Luohe Formation in the Ordos Basin: A Case Study of Outcrops in Longzhou Township, Jingbian County. *Glob. Geol.* **2018**, *37*, 702–711. [CrossRef]

11. He, Z.B.; Hu, B.Q.; Ji, H.L.; He, F.; Geng, Y.Y.; Huang, S.H.; Zhu, M.H. Geochemical Characteristics of Lower Cretaceous Sandstones in the Zhenyuan Area of the Ordos Basin and Their Implications for Provenance and Tectonic Setting. *Geol. Rev.* **2024**, *70*, 1291–1313. [CrossRef]
12. Feng, Y.; Ren, Y.; Xia, F.; Jiang, T.; Lu, F.; Guo, J. Study on the Early Cretaceous fluvial–desert sedimentary paleogeography in the northwest of the Ordos Basin. *Open Geosci.* **2023**, *15*, 20220469. [CrossRef]
13. Guo, Y.Q.; Li, B.Q.; Li, B.; Li, W.-H.; Cao, H.-X.; Liao, Y.; Wu, Z.-Z.; Fei, S.-X.; Zhang, Q.; Chen, Q.; et al. Sedimentary System and Palaeogeographic Evolution of the Ordos Basin, Northern China. *J. Palaeogeogr.* **2025**, *14*, 501–534. [CrossRef]
14. Makeen, Y.M.; Abdullah, W.H.; Ayinla, H.A.; Shan, X.; Liang, Y.; Su, S.; Noor, N.M.; Hasnan, H.K.; Asiwaju, L. Organic Geochemical Characteristics and Depositional Setting of Paleogene Oil Shale, Mudstone and Sandstone from Onshore Penyu Basin, Chenor, Pahang, Malaysia. *Int. J. Coal Geol.* **2019**, *207*, 52–72. [CrossRef]
15. Li, D.L. Geochemical Characteristics and Paleo-Sedimentary Environment Analysis of Oil Shale in the Chang 7 Member of the Triassic Yanchang Formation in the Southern Ordos Basin. Master's Thesis, Chang'an University, Xi'an, China, 2018. Available online: http://219.217.72.37:8088/KCMS/detail/detail.aspx?dbcode=CDFD&dbname=CDFD2019&filename=1018792429.nh (accessed on 14 January 2026).
16. Cullers, R.L. The Geochemistry of Shales, Siltstones and Sandstones of Pennsylvanian–Permian Age, Colorado, USA: Implications for Provenance and Metamorphic Studies. *Lithos* **2000**, *51*, 181–203. [CrossRef]
17. Cai, Y.; Ouyang, F.; Luo, X.; Zhang, Z.; Wen, M.; Luo, X.; Tang, R. Geochemical Characteristics and Constraints on Provenance, Tectonic Setting, and Paleoweathering of Middle Jurassic Zhiluo Formation Sandstones in the Northwest Ordos Basin, North-Central China. *Minerals* **2022**, *12*, 603. [CrossRef]
18. de Oliveira Carvalho, M.; Mottram, C.M.; de Morisson Valeriano, C.; Ramos, R.R.C.; Parrish, R.; Dunlop, J.; Cota, N.; Paravidini, G.; Neto, C.C.A.; Heilbron, M.; et al. Sedimentary Provenance in Continental Rifts: U–Pb Detrital Zircon, Nd and Sr Isotopes and Lithogeochemistry of the Eocene Alluvial Sandstones of the Resende Basin, SE–Brazil. *Sediment. Geol.* **2023**, *453*, 106452. [CrossRef]
19. Basu, A.; Bickford, M.E.; Deasy, R. Inferring Tectonic Provenance of Siliciclastic Rocks from Their Chemical Compositions: A Dissent. *Sediment. Geol.* **2016**, *336*, 26–35. [CrossRef]
20. Blaxland, A.B. Geochemistry and Geochronology of Chemical Weathering, Butler Hill Granite, Missouri. *Geochim. Cosmochim. Acta* **1974**, *38*, 843–852. [CrossRef]
21. Bhatia, M.R. Plate Tectonics and Geochemical Composition of Sandstones. *J. Geol.* **1983**, *91*, 611–627. [CrossRef]
22. Roser, B.P.; Korsch, R.J. Determination of Tectonic Setting of Sandstone–Mudstone Suites Using SiO_2 Content and K_2O/Na_2O Ratio. *J. Geol.* **1986**, *94*, 635–650. [CrossRef]
23. Lei, K.Y.; Liu, C.Y.; Zhang, L.; Wu, B.L.; Cun, X.N.; Sun, L. Element Geochemical Characteristics of the Jurassic Mudstones in the Northern Ordos Basin: Implications for Tracing Sediment Sources and Paleoenvironment Restoration. *Acta Sedimentol. Sin.* **2017**, *35*, 621–636. [CrossRef]
24. Zhang, T.F.; Sun, L.X.; Zhang, Y.; Chen, Y.H.; Li, Y.F.; Ma, H.L.; Lu, C.; Yang, C.; Guo, G.W. Geochemical Characteristics of Trace and Rare Earth Elements in Jurassic Yan'an Formation and Zhiluo Formation Mudstones from the Northern Margin of the Ordos Basin and Their Significance in Paleo-Sedimentary Environment. *J. Geol.* **2016**, *90*, 3454–3472. Available online: https://www.geojournals.cn/dzxb/dzxb/article/abstract/2016527?st=search (accessed on 19 January 2026).
25. Lu, Y.S.; Hu, Y.; Hou, Y.D.; Sun, J.F.; He, W.X.; Gao, X.Y.; Si, J.; Song, W.X. Geochemical Characteristics of Trace Elements and Their Implications for Sedimentary Environments in the Yanghugou Formation on the Western Margin of the Ordos Basin. *Sci. Technol. Eng.* **2021**, *21*, 11999–12009. Available online: http://www.stae.com.cn/uploadfile/cover/jsygc/2021_28_contents.pdf (accessed on 19 January 2026).
26. Sun, K.; Fan, L.; Xia, Y.; Li, C.; Chen, J.; Gao, S.; Wu, B.; Peng, J.; Ji, Y. Impact of Coal Mining on Groundwater of Luohe Formation in Binchang Mining Area. *Int. J. Coal Sci. Technol.* **2021**, *8*, 88–102. [CrossRef]
27. Cheng, X.Y.; Zhang, T.F.; Miao, P.S.; Cheng, Y.H.; Li, J.G.; Ao, C.; Xiao, R.G. Detrital Zircon U-Pb Geochronology of Uranium-Bearing Sandstone in the Lower Member of the Luohe Formation on the Southwestern Margin of the Ordos Basin: Implications for Lithospheric Extension. *Geol. China* **2023**, *50*, 853–871. [CrossRef]
28. Fan, L.M.; Shen, T. Gas Geological Conditions of Coal Mines on the Southwestern Margin of the Ordos Basin. *Coal Geol. China* **2011**, *23*, 18–23. Available online: https://m.doc88.com/p-0873767410018.html (accessed on 21 January 2026).
29. Yang, Y.Y.; Zhang, Y.L.; Hou, G.C. Sedimentary Facies Distribution and Basin Evolution Law of the Ordos Cretaceous Artesian Basin. *Acta Geosci. Sin.* **2008**, *29*, 405–413. [CrossRef]
30. Wang, K. Study on Tectonic Features and Natural Gas Preservation Conditions of the Lower Paleozoic in the Southern Ordos Basin. Master's Thesis, Northwest University, Xi'an, China, 2021. [CrossRef]
31. Xie, Y.; Wang, J.; Yin, Y.P.; Wu, X.M.; Wen, D.G.; Jiang, X.S.; Luo, J.N.; Wei, L.W.; Zheng, W.M. A Preliminary Study on Sedimentology of the Cretaceous Aquifer in the Ordos Basin. *Geol. Bull. China* **2003**, *22*, 818–828.

32. Liu, P.F.; Fan, J.T.; Guo, X.D. Research on Geological Characteristics and Influencing Factors of Coal Beds in Xiaozhuang Well Field. *Unconv. Oil Gas* **2018**, *5*, 31–40. Available online: https://m.doc88.com/p-9721740082982.html (accessed on 16 January 2026).
33. *SY/T 5368-2016*; Identification for Thin Section of Rocks. Standards Press of China: Beijing, China, 2016.
34. *GB/T 14506.28-2010*; Methods for Chemical Analysis of Silicate Rocks—Part 28. Standards Press of China: Beijing, China, 2010.
35. *GB/T 14506.30-2010*; Methods for Chemical Analysis of Silicate Rocks—Part 30. Standards Press of China: Beijing, China, 2010.
36. Passega, R.; Byramjee, R. Grain-size image of clastic deposits. *Sedimentology* **1969**, *13*, 233–252. [CrossRef]
37. Buller, A.T.; Mcmanus, J. The application of quartile deviation-median diameter curves to the interpretation of sedimentary rocks. *J. Geol. Soc.* **1974**, *130*, 79–83. [CrossRef]
38. Boynton, W.V. Cosmochemistry of Rare Earth Elements: Meteorite Studies. In *Rare Earth Element Geochemistry: Developments in Geochemistry*; Henderson, P., Ed.; Elsevier: Amsterdam, The Netherlands, 1984; Volume 2, pp. 63–114. [CrossRef]
39. Song, K.; Lü, J.W.; Du, J.L.; Wang, H.K. Provenance Analysis and Delta Sedimentary System of the Upper Triassic Yanchang Formation in the Central Ordos Basin. *J. Palaeogeogr.* **2002**, *4*, 59–66. Available online: http://219.217.72.37:8088/KCMS/detail/detail.aspx?dbcode=CJFD&dbname=cjfd2002&filename=GDLX200203007 (accessed on 21 January 2026).
40. McLennan, S.M.; Hemming, S.; McDaniel, D.K.; Hanson, G.N.; Johnsson, M.J.; Basu, A. Geochemical Approaches to Sedimentation, Provenance, and Tectonics. *Spec. Pap. Geol. Soc. Am.* **1993**, *284*, 21–40. [CrossRef]
41. Bhatia, M.R.; Crook, K.A. Trace Element Characteristics of Graywackes and Tectonic Setting Discrimination of Sedimentary Basins. *Contrib. Mineral. Petrol.* **1986**, *92*, 181–193. [CrossRef]
42. Gu, X.X.; Liu, J.M.; Zheng, M.H.; Tang, J.; Qi, L. Provenance and Tectonic Setting of the Proterozoic Turbidites in Hunan, South China: Geochemical Evidence. *J. Sediment. Res.* **2002**, *72*, 393–407. [CrossRef]
43. Floyd, P.A.; Leveridge, B.E. Tectonic Environment of the Devonian Gramscatho Basin, South Cornwall: Framework Mode and Geochemical Evidence from Turbiditic Sandstones. *J. Geol. Soc. Lond.* **1987**, *144*, 531–542. [CrossRef]
44. Lerman, A. *Lakes: Chemistry, Geology, Physics*; Springer: Berlin/Heidelberg, Germany, 1978; pp. 79–83. [CrossRef]
45. Chen, J.; Wang, Y.J.; Chen, Y.; Liu, L.; Ji, J.; Lu, H. Geochemical Characteristics of Rb and Sr in Chinese Loess Strata and Their Implications for Paleomonsoon Climates. *Acta Geol. Sin.* **2000**, *75*, 259–266. [CrossRef]
46. Degens, E.T.; Williams, E.G.; Keith, M.L. Environmental Studies of Carboniferous Sediments, I. Geochemical Criteria for Differentiating Marine from Fresh-Water Shales. *AAPG Bull.* **1957**, *41*, 2427–2455. [CrossRef]
47. Virgo, D. Partition of Strontium between Coexisting K-Feldspar and Plagioclase in Some Metamorphic Rocks. *J. Geol.* **1968**, *76*, 331–346. [CrossRef]
48. Grocolas, T.; Bloch, E.M.; Bouvier, A.S.; Müntener, O. Diffusion of Sr and Ba in plagioclase: Composition and silica activity dependencies, and application to volcanic rocks. *Earth Planet. Sci. Lett.* **2025**, *651*, 119141. [CrossRef]
49. Samanta, S.; Goswami, M.C.; Baidya, T.K.; Mukherjee, S.; Dey, R. Mineralogy and carbothermal reduction behaviour of vanadium-bearing titaniferous magnetite ore in Eastern India. *Int. J. Miner. Metall. Mater.* **2013**, *20*, 917–924. [CrossRef]
50. Jones, B.J.; Manning, A.C. Comparison of Geochemical Indices Used for the Interpretation of Palaeoredox Conditions in Ancient Mudstones. *Chem. Geol.* **1994**, *111*, 111–129. [CrossRef]
51. Schaltegger, U.; Fanning, C.M.; Günther, D.; Maurin, J.C.; Schulmann, K.; Gebauer, D. Growth, annealing and recrystallization of zircon and preservation of monazite in high-grade metamorphism: Conventional and in-situ U-Pb isotope, cathodoluminescence and microchemical evidence. *Contrib. Mineral. Petrol.* **1999**, *134*, 186–201. [CrossRef]
52. Kimura, H.; Watanabe, Y. Ocean Anoxia at the Precambrian–Cambrian Boundary. *Geology* **2001**, *29*, 995–998. [CrossRef]

Disclaimer/Publisher's Note: The statements, opinions and data contained in all publications are solely those of the individual author(s) and contributor(s) and not of MDPI and/or the editor(s). MDPI and/or the editor(s) disclaim responsibility for any injury to people or property resulting from any ideas, methods, instructions or products referred to in the content.